


# Influence of CO<sub>2</sub>-Rich Syngas on the Selectivity to C<sub>10</sub>–C<sub>14</sub> in a Coupled Fischer-Tropsch/Hydrocracking Process

Tabea J. Stadler<sup>1</sup>, Barbara Bertin-Mente<sup>1</sup>, Roland Dittmeyer<sup>1</sup>, Lucas T. Brübach<sup>1</sup>, Tim Böltken<sup>2</sup>, and Peter Pfeifer<sup>1,2,\*</sup>

DOI: 10.1002/cite.202100172

 This is an open access article under the terms of the Creative Commons Attribution-NonCommercial License, which permits use, distribution and reproduction in any medium, provided the original work is properly cited and is not used for commercial purposes.

*Dedicated to Prof. Dr. Thomas Hirth on the occasion of his 60th birthday*

Synthesis gas (syngas) used for the production of synthetic fuels may contain significant amounts of CO<sub>2</sub>, depending on its source. For Fischer-Tropsch synthesis on cobalt, CO<sub>2</sub> can be considered as inert diluent. However, in the specific case of a coupled Fischer-Tropsch-hydrocracking (FT-HC) process, CO<sub>2</sub> could interact with the catalyst in the HC step. In this experimental study, HC product distributions obtained for FT-syngas compositions with and without CO<sub>2</sub> and N<sub>2</sub> are presented. The selected feed gas compositions result from an advanced syngas production route via plasma splitting of CO<sub>2</sub>. Main target product was kerosene, here being defined as C<sub>10</sub>–C<sub>14</sub>. It was found that the CO<sub>2</sub> presence is negligible with regard to adsorption or reaction on the HC catalyst. Further insights into possible impacts of CO<sub>2</sub> could be obtained from the analysis of alcohols in the aqueous phase.

**Keywords:** CO<sub>2</sub>-rich syngas, Fischer-Tropsch synthesis, Hydrocracking, Plasma splitting of CO<sub>2</sub>, Power-to-fuels

*Received:* September 10, 2021; *revised:* October 14, 2021; *accepted:* December 13, 2021

## 1 Introduction

Carbon neutral synthetic fuels are among the most promising alternatives for the successful defossilization of the transport sector [1]. Since not all means of transport can manage without liquid fuels due to gravimetric or volumetric restrictions, so-called Power-to-Liquid (PtL) processes are emerging technologies. The Kerogreen project aims to investigate a compact PtL conversion route from water and captured CO<sub>2</sub> to carbon neutral aviation fuel powered by renewable energy sources [2]. Here, CO<sub>2</sub> is activated to CO in a plasma splitting reactor combined with O<sub>2</sub> separation in a solid oxide electrolyte cell [3]. CO is partly converted back to CO<sub>2</sub> with steam in order to produce synthesis gas, a mixture of CO + H<sub>2</sub> (syngas), via the water-gas shift reaction. The by-product CO<sub>2</sub> is removed and recovered in situ through a sorption-enhanced process (SEWGS) [4]. Syngas reacts subsequently in a Fischer-Tropsch (FT) reactor followed by a hydrocracking (HC) reactor to produce primarily hydrocarbons in the middle distillate range. Therefore, it is important to know if certain concentrations of CO<sub>2</sub> in the syngas influence the product composition in this process, since also further upgrading steps are necessary with the hydrotreated crude to meet the fuel quality regulations for direct use as synthetic kerosene [5–7].

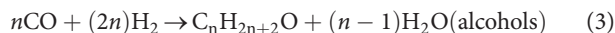
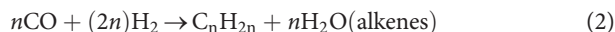
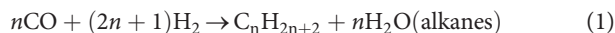
Compact, decentralized PtL concepts, such as the Kero-green process but also others in general, do not only require a modification of the FT process but also of the product upgrading steps in terms of simplicity and conditions. Commercial HC processes are firstly not applicable in a compact coupled FT-HC process layout due to pure H<sub>2</sub> requirement and, secondly, they cannot be economically scaled down so far [8]. One possibility to overcome this issue is the direct coupling of the HC reactor into the synthesis gas loop of the FT. The HC reaction is then conducted under FT conditions, i.e., in presence of CO. In any case of CO<sub>2</sub> in the syngas, also the CO<sub>2</sub> contribution towards process performance gains interest. Advantages and disadvantages of the direct coupling are discussed in the subsequent paragraphs.

<sup>1</sup>Tabea J. Stadler, Barbara Bertin-Mente, Prof. Dr.-Ing. Roland Dittmeyer, Lucas T. Brübach, Prof. Dr.-Ing. Peter Pfeifer  
peter.pfeifer@kit.edu

Karlsruhe Institute of Technology (KIT), Institute for Micro Process Engineering (IMVT), Hermann-von-Helmholtz-Platz 1, 76344 Eggenstein-Leopoldshafen, Germany.

<sup>2</sup>Dr.-Ing. Tim Böltken, Prof. Dr.-Ing. Peter Pfeifer  
INERATEC – Innovative Chemical Reactor Technologies GmbH, Siemensallee 84, 76187 Karlsruhe, Germany.

The FT synthesis is a heterogeneously catalyzed, polymerization-like exothermic hydrogenation reaction and converts syngas to a hydrocarbon mixture and water [9]. The hydrocarbon product consists of a variety of species with up to 100 carbon atoms and can be denoted as synthetic crude (syncrude). FT carried out with cobalt-based catalysts at low temperatures (200–250 °C, Co-LTFT) produces mainly linear alkanes (Eq. (1)), but also alkenes (Eq. (2)) and minor quantities of oxygenates, such as alcohols (Eq. (3)) [10].



The product distribution on a weight basis can be approximated by means of the Anderson-Schulz-Flory distribution (ASF, Eq. (4)) [11, 12].

$$w_{\text{ASF},n_{\text{C}_i}} = n_{\text{C}_i}(1 - \alpha)^2 \alpha^{(n_{\text{C}_i}-1)} \quad (4)$$

A graphical illustration of the ASF product distribution is depicted in Fig. 1. The chain growth probability  $\alpha$  is defined as the ratio of propagation to the sum of propagation and termination and depends on the reaction conditions and catalyst. Typical Co-LTFT  $\alpha$  values range from 0.88 to 0.95 [13]. According to Eq. (4), the primary selectivity towards kerosene (here being defined as  $\text{C}_{10}$ – $\text{C}_{14}$ ) is limited to a theoretical maximum of 23 % for  $\alpha = 0.84$ . To overcome this limitation, the product distribution must be narrowed with adequate upgrading processes. Assuming complex refining technologies at large scale, an industrial LTFT jet fuel refinery can yield up to 57 % jet fuel from syncrude [14].

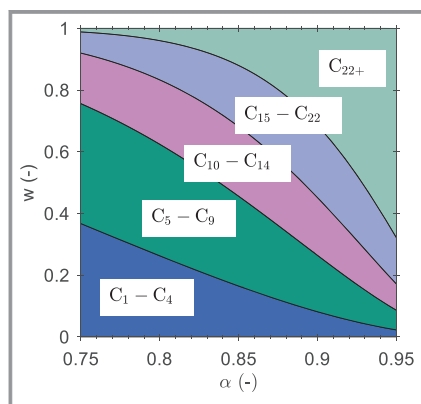


**Figure 1.** ASF syncrude composition for lumped product groups:  $\text{C}_1$ – $\text{C}_4$ , gases;  $\text{C}_5$ – $\text{C}_9$ , naphtha;  $\text{C}_{10}$ – $\text{C}_{14}$ , kerosene;  $\text{C}_{15}$ – $\text{C}_{22}$ , gas oil;  $\text{C}_{22+}$ , waxes.

HC is among the most relevant refinery processes for the conversion of long-chain hydrocarbons to mainly middle distillates with naphtha as by-product. It promotes skeletal

isomerization of  $n$ -alkanes to isoalkanes to enhance the cold flow properties of the resulting synthetic fuel. HC is carried out on bifunctional catalysts with de/hydrogenation and cracking functionality. On the metal sites of the catalyst, alkanes are dehydrogenated to alkenes. On the Brønsted acid sites, these alkenes are protonated to form alkylcarbenium ions and undergo isomerization and scission reactions of the carbon-carbon bonds. The products desorb from the acid sites and unsaturated alkenes can further be hydrogenated on the metal sites. Ideal hydrocracking (Eq. (5)) occurs if the de/hydrogenation and the cracking functionality are properly balanced so that secondary cracking becomes negligible [15]. HC is typically performed under elevated pressure (35 to 70 bar) and temperature (325 to 375 °C). In direct combination with FT, “mild” HC with lower pressure and temperature can be applied [16, 17]. On the one hand, this lower pressure and lower temperature is beneficial with regard to the process efficiency since no compression or considerable heating-up of the product gas and liquid flow are required. On the other hand, noble metals are required for the carbenium ion formation and hydrogenation steps, which are partly blocked due to competitive adsorption of CO. This may lead to secondary cracking and, thus, to a potential negative impact on middle distillate yield.



Many studies reported on the influence of  $\text{CO}_2$ -rich feeds in Co-LTFT [18–21]. The majority concluded that  $\text{CO}_2$ , which is, e.g., contained in significant amounts in biomass-derived syngas, acts mainly as diluent on Co catalysts. However, the influence of  $\text{CO}_2$  on coupled FT-HC processes has received less attention in literature although it may be a serious parameter in a case of process integration.

Therefore, this experimental study aims to understand the impact of a possible slip of  $\text{CO}_2$ .  $\text{CO}_2$  could originate from incomplete separation in the SEWGS reactor (for a detailed process description, see [4]), and thus, influence the subsequent process steps and product quality in the Kerogreen process chain. Various syngas compositions were fed to an FT reactor coupled with an HC reactor cascade. The weight hourly space velocity ( $WHSV_{\text{FT}}$ , Eq. (12)) as well as the CO conversion ( $X_{\text{CO}}$ , Eq. (6)) in the FT were kept constant. The following cases were investigated: syngas with low  $\text{CO}_2$  dilution (incomplete  $\text{CO}_2$  removal in the SEWGS reactor) and with high  $\text{CO}_2$  dilution (no  $\text{CO}_2$  removal in the SEWGS reactor), and for comparative purposes: syngas with equivalent  $\text{N}_2$  dilution and without dilution.

## 2 Materials and Methods

### 2.1 Reactors and Catalysts

The experiments were conducted in a micro-structured FT reactor coupled with an HC reactor cascade consisting of three identical tubular reactors in sequence, see also [22].

A commercial Co-based catalyst was used for low-temperature FT (spheres with a diameter of 50–200  $\mu\text{m}$ ). In the HC reactor cascade, bifunctional Pt/H-ZSM-5 (0.5 wt % Pt) catalyst extrudates (1/16"  $\times$  3 mm) were employed.

## 2.2 Experimental Setup

Fig. 2 shows a simplified process scheme of the experimental setup used in this study. The feed gases  $\text{H}_2$ ,  $\text{CO}$ ,  $\text{CO}_2$ , and  $\text{N}_2$  were provided by a central gas supply and fed into the system by calibrated mass flow controllers (Brooks Instrument, USA). 5 vol % of the total flow passed through a permanent bypass to enable continuous feed control in the online gas chromatograph (GC). The electrically preheated gases entered the reaction channels of the evaporation-cooled FT reactor (INERATEC GmbH, Germany) [22–24].

The reaction channels of the FT reactor were filled with catalyst and adjacent cooling channels ensure precise temperature control. Preheated water entered the cooling channels, evaporated by consuming the reaction heat, and left the reactor as two-phase flow. Temperature adjustment in the reactor was realized by means of the boiling point, which could be adjusted by the pressure in the water cycle. This technology results in nearly isothermal reaction conditions. Electrical heating cartridges alongside the reactor provided additional heat for the start-up of the reaction and compensated heat losses at the outer walls. The reactor itself was placed in a box filled with insulation material to reduce heat losses. Type K thermocouples in the water cycle as well as in the reactor inlet and outlet, and at various positions between the channels were used to monitor the temperatures. An automated shutdown routine implemented in the process control system (LabView, National Instruments, USA) ensured safe operation conditions.

The product flow leaving the FT reactor could either be directed to the product separation unit (hot and cold trap) for analysis or to the HC reactor cascade for further pro-

cessing. Due to their interconnections, the number of operating HC reactors could be adjusted manually. Additional gas could optionally be dosed into the HC section. The temperature of each tubular HC reactor (inner diameter: 14 mm, length: 102 mm) was regulated by a heating jacket and monitored internally by a K-type thermocouple located inside the catalyst bed. The whole reactor cascade was placed in a box filled with insulation material to reduce heat losses.

Products from FT or coupled FT-HC were fed into the hot trap under pressure. The hot trap was electrically heated to a constant temperature of 180  $^\circ\text{C}$ . Long-chain hydrocarbons (the wax fraction) condense and accumulate here. The remaining parts of the product moved on to the cold trap which was cooled to 10  $^\circ\text{C}$ . Here, the oil and water fraction condensed. To ensure that no water condensation occurred in the hot trap, thus leading to under-estimation of alcohols in the water phase of the cold trap, the hot trap temperature was set sufficiently high [23]. Wax, oil, and water fraction were analyzed in offline GCs. The non-condensed gases were analyzed in an online GC and left the system through an exhaust line.

A back-pressure regulator (BSH series, Swagelok, USA) controlled the system pressure. Unwanted condensation and wax plugging in the tubes was prevented by electrical heating coils.

## 2.3 Product Analysis and Data Evaluation

The feed and gaseous product flows were analyzed online in a GC (7890B, Agilent Technologies, customized by Teckso GmbH, Germany) equipped with two thermal conductivity detectors (TCD1, TCD3) and one flame ionization detector (FID).  $\text{H}_2$ ,  $\text{CH}_4$ ,  $\text{CO}$ , and  $\text{N}_2$  were detected by TCD1 after being separated on a micropacked HayeSep Q and a mole sieve 5A column.  $\text{CO}_2$  and hydrocarbons (up to  $\text{C}_7$ ) were separated on a HP-Plot/Q column (all columns: Agilent Technologies, USA) and detected by TCD3 and the FID, respectively. Ar was used as carrier gas and  $\text{N}_2$  as internal standard.

Water and oil phase gathered in the cold trap were separated in a separation funnel. Both phases were analyzed offline in a GC (7820A, Agilent Technologies, USA) equipped with an Rtx-1 column (60 m, 0.32 mm, 1  $\mu\text{m}$ , Restek, USA) and an FID. Acetonitrile was added as internal standard to the water phase for the quantification of alcohols ( $\text{C}_1$ – $\text{C}_5$ ). The oil phase (hydrocarbons:  $\sim\text{C}_4$ – $\text{C}_{27}$ ) was injected without a solvent by an auto-

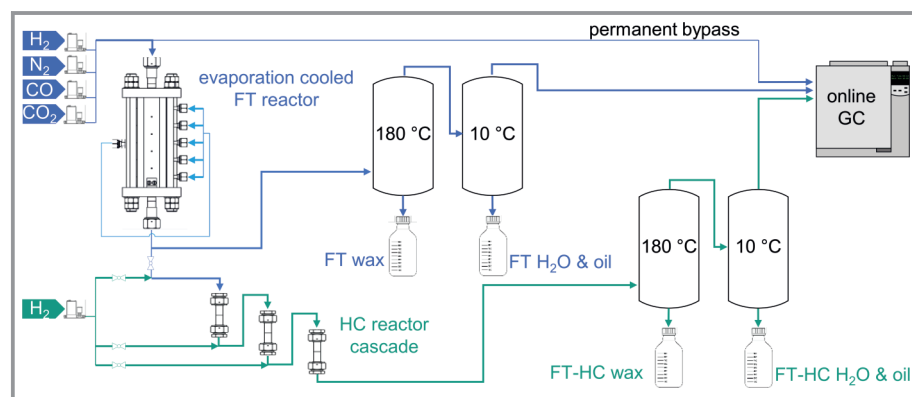


**Figure 2.** Simplified flow scheme of the experimental setup. Feed gases enter the micro-structured FT reactor and can optionally be fed to the HC reactor cascade. Products are separated in a wax phase (hot trap), liquid (oil and water) phase (cold trap), and remaining gases.

matic liquid sampler. It was analyzed quantitatively with a 100-% method under the assumption of a constant relative response factor. This is usually justified for aliphatic hydrocarbon mixtures without heteroatoms [25].

The composition of the long-chain hydrocarbons in the wax fraction ( $\sim C_{10}$ – $C_{60}$ ) was determined offline in a high-temperature GC (7890B, Agilent Technologies, USA) equipped with a MXT-1 column (30 m, 0.53 mm, 0.25  $\mu$ m, Restek, USA) and a high temperature FID. The dissolved wax sample (200 mg wax dissolved in 20 mL cyclohexane, ultrasound bath at 40 °C) was directly injected into the temperature programmable inlet (Da Vinci Laboratory Solutions B.V., The Netherlands) to avoid discrimination of high-boiling components.

The conversion of CO  $X_{CO}$  was calculated according to Eq. (6).

$$X_{CO} = \frac{\dot{n}_{CO,in} - \dot{n}_{CO,out}}{\dot{n}_{CO,in}} \quad (6)$$

Wax, water, and oil samples collected under steady-state conditions were weighted for integral mass flow  $\dot{m}$  determination. Mass fraction  $w$  of hydrocarbon  $i$  and carbon monoxide related selectivity  $S$  towards hydrocarbon  $i$  were calculated according to Eqs. (7) and (8), respectively. The average chain length  $\bar{n}_C$  was derived from Eq. (9). As far as analytically feasible, it was further distinguished between  $n$ -alkanes and 1-alkenes [26]. The  $n$ -alkane fraction  $a$  of hydrocarbon  $i$  is calculated according to Eq. (10). The conversion of long-chained hydrocarbons ( $n_C > 22$ )  $X_{C_{22+}}$  in the HC reactor resulted from Eq. (11).

$$w_i = \frac{\dot{m}_{i,out}}{\sum \dot{m}_{i,out}} \quad (7)$$

$$S_{i,CO} = \frac{\dot{n}_{i,out}}{\dot{n}_{CO,in} - \dot{n}_{CO,out}} n_{C,i} \quad (8)$$

$$\bar{n}_C = \sum (w_i n_{C,i}) \quad (9)$$

$$a_i = \frac{\dot{n}_{i,n\text{-alkane}}}{\dot{n}_i} \quad (10)$$

$$X_{C_{22+}} = \frac{\frac{X_{CO,FT-HC}}{X_{CO,FT}} \sum (\dot{n}_{C_{22+,FT,out}} n_{C,i}) - \sum (\dot{n}_{C_{22+,FT-HC,out}} n_{C,i})}{\frac{X_{CO,FT-HC}}{X_{CO,FT}} \sum (\dot{n}_{C_{22+,FT,out}} n_{C,i})} \quad (11)$$

## 2.4 Experimental Procedure

### 2.4.1 Reduction and Pre-Conditioning

Prior to the experiments, both catalysts were reduced in situ in  $H_2$  atmosphere (FT: 100 %  $H_2$ , 320 °C, 16 h; HC: 10 %  $H_2$  in  $N_2$ , 300 °C, 5 h). A run-in phase of 500 h ensured stable catalyst activity. Typical initial degradation due to wax formation in the catalyst pores requires  $\sim 70$  h according to preliminary studies. To observe possible catalyst deactivation, a reference point was repeatedly analyzed during the measurement campaign; the conversion remained constant within the noise of analytics of  $\pm 2$  %.

### 2.4.2 FT and FT-HC Coupling Experiments

The system pressure was set to 20 bar for all experiments. The reaction temperature in the FT reactor was adjusted to maintain a constant CO conversion in all experiments between 195 and 200 °C. The reaction temperature in the HC reactor cascade was set to 230 °C.

The experimental nomenclature was chosen in the following order: “Dil” for dilution of the syngas with “ $N_2$ ” or “ $CO_2$ ” followed by a numbering with the concentration level “1” or “2” followed by “A” or “B” for variation of other parameters (number of HC stages and hydrogen addition to the HC feed) used in the experiment. “FT” and “HC” at the end indicate whether the product is derived from FT or from the coupled FT-HC process. An exception from the nomenclature is the experiment “Ref\_A” which indicates an undiluted syngas for “FT” or coupled process “HC”. The specific conditions are provided in the following tables and paragraphs.

Fig. 3 shows the ramp-up of an individual experimental point with regard to reaction temperatures in FT and HC stages and conversion in the FT reactor. The process conditions for every experimental point were kept constant for about 24 h in the FT reactor to accomplish steady state in

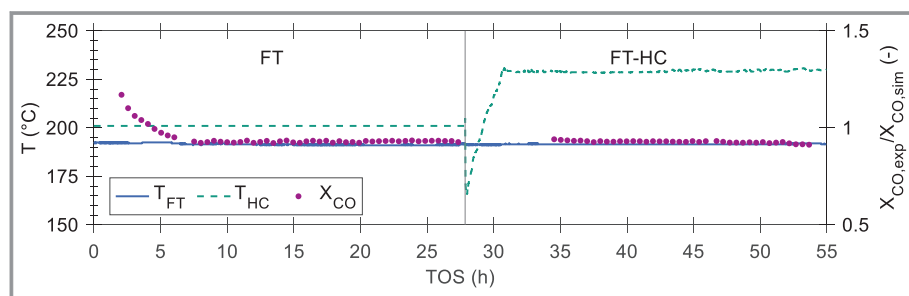


**Figure 3.** Exemplary experimental curve for FT-HC coupling experiment (Dil\_CO2\_1).

the individual run, and FT reference samples were collected for at least 3 h at the end of that period in the traps. For the FT-HC coupling, the FT effluent was slowly redirected to the pressurized and preheated HC reactor cascade. The cascade was flushed for at least 30 min to ensure the build-up of a wax layer on the catalyst pellets. Then, the HC reactors were heated to target temperature (230 °C). After about 24 h, steady-state HC samples were taken out of the traps (collection time ~3 h). The graph in Fig. 3 indicates that the FT reactor has reached steady-state reaction conditions in the run-in phase and also during ramp-up. During the FT reference measurement, the HC reactor cascade was flushed with an H<sub>2</sub>/N<sub>2</sub> mixture to avoid possible catalyst oxidation and pressure surge.

The CO conversion plotted in Fig. 3 is normalized to simulated CO conversion. Simulated values were derived from an INERATEC in-house MATLAB<sup>®</sup> program, which was fitted to a simplified version of the Visconti model [27] with data points obtained in a smaller oil-cooled reactor as used elsewhere [28] and which has been approved by many data points before. The activation energies in the model parameter set are slightly lower and the rate constants are in the order of 7–10 higher than in the original publication of Visconti et al. due to the applied highly active catalyst.

FT inlet conditions for all experiments are summarized in Tab. 1. Nitrogen was used as diluent and (partly) replaced in two runs with CO<sub>2</sub> while the reference run was performed with only 3 % N<sub>2</sub> as internal standard. Typically, the weight hourly space velocity in the FT reactor  $WHSV_{FT}$  was kept constant (Eq. (12)).

$$WHSV_{FT} = \frac{\dot{m}_{in}}{m_{cat,FT}} \quad (12)$$

**Table 1.** FT feed in the FT-HC coupling experiments. System pressure: 20 bar; H<sub>2</sub>/CO ratio: 2; FT catalyst mass/HC catalyst mass: 7.4; temperature in FT: 195–200 °C (adjusted to maintain constant CO conversion); no additional gas feed to HC; temperature in HC: 230 °C.

	H <sub>2</sub> [%]	CO [%]	CO <sub>2</sub> [%]	N <sub>2</sub> [%]	$WHSV_{FT}$ [h <sup>-1</sup> ]
Dil_N2	38.8	19.4	0	41.8	4.5
Dil_CO2_1	38.8	19.4	38.8	3.0	4.5
Dil_CO2_2	38.8	19.4	5.0	36.8	4.5
Ref_A	64.7	32.3	0	3	3.5 <sup>a)</sup>

a) The desired value of 4.5 was not reachable due to experimental restrictions.

### 2.4.3 Variation of HC Reaction Conditions

To further investigate the influence of CO<sub>2</sub> on HC, two modifications in the HC were tested with identical FT product as feed: 1) additional H<sub>2</sub> feed in the HC, and 2) reduction of HC catalyst mass (Tab. 2).

**Table 2.** Variation of HC conditions. FT feed equal to Dil\_CO2\_1 (Tab. 1). Temperature in HC: 230 °C.

	H <sub>2</sub> HC [mL <sub>N</sub> min <sup>-1</sup> ]	$m_{cat,FT}/m_{cat,HC}$ [-]
Dil_CO2_1	0	7.4
Dil_CO2_1A	500	7.4
Dil_CO2_1B	500	11.1

## 3 Results and Discussion

In this section, hydrocarbons were classified according to their carbon number and grouped into lumps: C<sub>1</sub>–C<sub>4</sub>: gases, C<sub>5</sub>–C<sub>9</sub>: naphtha, C<sub>10</sub>–C<sub>14</sub>: kerosene, C<sub>15</sub>–C<sub>22</sub>: gas oil, C<sub>22+</sub>: waxes. The main target product was kerosene, here being defined as C<sub>10</sub>–C<sub>14</sub> [14]. Further insights into possible impacts of CO<sub>2</sub> could be obtained from the analysis of alcohols in the aqueous phase.

Concluding from the high reproducibility of the reference point in both reactors, FT and HC, no significant catalyst deactivation occurred during the measurement campaign after the run-in phase. The total mass balance deviation was well below 3.5 % in all experiments. It was determined from the integral mass flow of the liquid and wax phase collected under steady-state conditions and continuous gas phase analysis.

### 3.1 FT Reference Measurements

Fig. 4 shows the carbon-based mass fractions for all FT reference measurements in form of an Anderson-Schulz-Flory (ASF) plot, i.e., the logarithmic of the weight fraction of the C-species divided by the respective C-number. For the C<sub>10</sub>–C<sub>50</sub> species, a product distribution, characterized by an averaged chain-growth probability of 0.91, is obtained. The

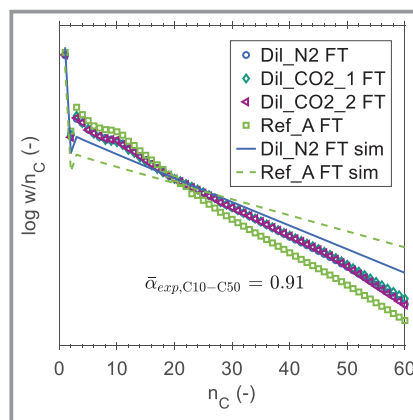


**Figure 4.** Experimental carbon-related mass fractions of hydrocarbons for FT reference measurements (Tab. 1) versus model prediction with the in-house MATLAB<sup>®</sup> code. Fitted average ASF chain growth probability for C<sub>10</sub>–C<sub>50</sub> (Eq. (4)).

chain growth probability was fitted according to Eq. (4) with  $R^2$  values above 0.99 for all individual fits. The modeling results are also plotted for the two reference points as lines.

For short-chain hydrocarbons ( $< C_{10}$ ), saddle-like deviations from the ideal ASF distribution emerge. These deviations might rather be explained by experimental artefacts than mechanistic effects [29]. One possible explanation might be found in the sampling procedure. The sampling of the liquid and wax phase included a release to ambient temperature and pressure. Hence, short chain hydrocarbons dissolved in the liquid and wax phase under reaction conditions could be irrecoverably lost to air due to a phase change into gas state. This flash loss could result in a dip as observed in the ASF plot [30]. This fact can lead to a deviation of the detected chain-growth probability in the range of 1–2% despite high quality fits and explain deviations from the modeling results. Nevertheless, the long-chain product fractions of interest do not seem to be influenced by the loss during liquid sampling.

Detailed information on the FT reference measurements is given in Tab. 3. The mass fractions for hydrocarbon lumps agree well with literature data for Co-LTFT [10]. Unfortunately, it was not possible to reach equal CO conversion in all experiments due to technical restrictions of the setup. The reference measurement without dilution (Ref\_A) exhibited significantly higher heat production and was run under less than half the desired conversion. This could explain the different product distribution for Ref\_A. The results show that no significant difference is observed between the product distribution obtained from syngas enriched with  $N_2$  and  $CO_2$ . As known from previous studies,  $N_2$  has no influence on the FT kinetics and serves as inert gas [31]. Thus, also  $CO_2$  does not play an influencing role in FT with the employed Co catalyst and acts mainly as diluent in the presence of CO. This observation is in line with various studies which stated that  $CO_2$  removal from raw syngas is not necessary for FT on Co catalysts [19–21, 32]. Visconti et al. attributed the inert behavior of  $CO_2$  in the presence of CO to competitive adsorption on the catalyst free sites [18]. An increase in methane selectivity due to  $CO_2$  was not expected for the investigated CO conversion range under constant  $H_2/CO$  feed ratio [33–35].

**Table 3.** Experimental conversion and mass fractions of hydrocarbon product lumps for FT reference measurements (Tab. 1), fitted ASF chain growth probability, and calculated kerosene ( $C_{10}$ – $C_{14}$ ) mass fraction.

	$X_{CO,exp,FT}/X_{CO,sim}$ [-]	$w_{C5-C9}$ [-]	$w_{C10-C14}$ [-]	$w_{C15-C22}$ [-]	$w_{C22+}$ [-]	$\alpha_{C10-C50}$ [-] <sup>a)</sup>	$w_{ASF,C10-C14}$ [-] <sup>b)</sup>
Dil_N2 FT	0.85	0.15	0.17	0.22	0.39	0.92	0.16
Dil_CO2_1 FT	0.93	0.14	0.17	0.21	0.40	0.92	0.16
Dil_CO2_2 FT	0.96	0.15	0.18	0.21	0.39	0.92	0.16
Ref_A FT	0.39	0.19	0.22	0.22	0.28	0.90	0.19

a) Fitted value:  $R^2 > 0.99$ ; b) Eq. (4) with determined chain growth probability.

### 3.2 Coupled FT-HC Measurements

In all FT-HC coupling experiments, a shift in the product distribution towards shorter hydrocarbons is clearly identified compared to the corresponding FT reference. The product distribution of one experimental point (Dil\_CO2\_1) is exemplarily shown in Fig. 5 in terms of the weight fractions of the C-species as function of the corresponding C-numbers. The net production of hydrocarbon species through the hydrocracking process is strictly limited to  $C_{14}$  in all experiments. Considering preliminary studies, this effect is mainly attributed to the shape selectivity of the employed H-ZSM-5 and gives rise to the occurrence of pore mouth cracking. Primarily produced long-chain hydrocarbons undergo secondary cracking reactions due to mass transfer limitations in the narrow pores of the zeolite.

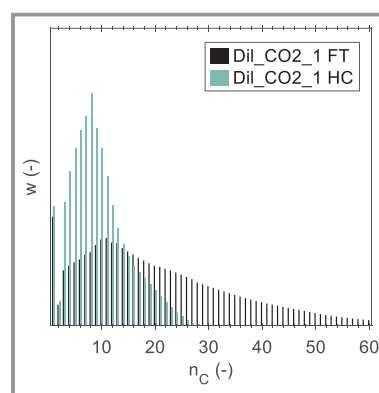


**Figure 5.** Hydrocarbon mass fractions for FT and coupled FT-HC measurement (Dil\_CO2\_1). FT feed: 38.8%  $H_2$ , 19.4%  $CO$ , 38.8%  $CO_2$ , 3.0%  $N_2$ ,  $WHSV_{FT} = 4.5 h^{-1}$ .

Minor deviations ( $< 2\%$ ) between the CO conversion of the FT reference measurement and the coupled FT-HC point were considered for the determination of the wax conversion (Eq. (11)). The results summarized in Tab. 4 do not indicate a correlation between the wax conversion and the ratio of gas velocity and FT product. All wax conversion rates are well above 75% and therefore quite high. However, the corresponding changes in boundary conditions for phase equilibrium influence the reaction conditions on the

**Table 4.** Experimental wax ( $C_{22+}$ ) conversion in coupled FT-HC measurements and average chain length for FT and FT-HC measurements (Tabs. 1 and 2).

	$X_{C_{22+},HC}$ [%]	$\bar{n}_{C,FT}$ [-]	$\bar{n}_{C,HC}$ [-]
Dil_N2	86.0	20	11
Dil_CO2_1	94.8	20	9
Dil_CO2_2	81.7	20	11
Ref_A	77.0	17	11

HC catalyst surface. More gas phase means that more heavy molecules may evaporate, and the probability of drying out of the liquid film on the catalyst increases. This would allow further secondary cracking, i.e., loss of the gas oil fraction. The average chain length decreased in the HC by 9 and 11 with diluted syngas feed ( $N_2$  and  $CO_2$ ), and by only 6 in the pure syngas feed experiment.

The integral product selectivity of the FT and FT-HC hydrocarbon product lumps is depicted in Fig. 6 for  $C_6$ – $C_9$  (naphtha),  $C_{10}$ – $C_{14}$  (kerosene),  $C_{15}$ – $C_{21}$  (gas oil), and  $C_{22+}$  (wax) to identify decrease and increase of these fractions. It is apparent that the wax fraction together with small parts of the gas oil fraction is selectively converted to kerosene and naphtha range hydrocarbons in the HC. A more detailed look at the product composition with respect to the  $n$ -alkane content in  $C_6$ – $C_9$  (naphtha),  $C_{10}$ – $C_{14}$  (kerosene), and  $C_{15}$ – $C_{21}$  (gas oil) is given in Fig. 7. Even though it is not possible to distinguish with normal GC analysis between isoalkanes and different molecules of alkenes and isoalkenes, it can be concluded that the  $n$ -alkane fraction in gas oil and kerosene is remarkably lower for all FT-HC products compared to the corresponding FT product, whereas the reverse effect occurs slightly for the waxes. These results indicate that linear FT alkanes were either successfully isomerized or dehydrogenated in the HC.

A high content of isoalkanes in the synthetic fuel is desirable as it enhances its cold flow properties, but any type of alkene is lowering the thermal stability and is therefore not allowed in the synthetic kerosene substitute. As the presence of CO and water in the HC feed heavily influences the catalyst behavior [36,37], the formation of mainly isoalkenes is nevertheless highly likely and a subsequent hydrogenation is required. The pure syngas feed (Ref\_A) showed similar trends as the diluted feed. No significant difference between the syngas feed with  $N_2$  (Dil\_N2) and  $CO_2$  (Dil\_CO2\_1 and Dil\_CO2\_2) could be deduced. Thus, the effects of dilution on the product distribution obtained in the coupled FT-HC process are negligible within the limited variations of parameters (i.e., upfront dilution and FT conver-

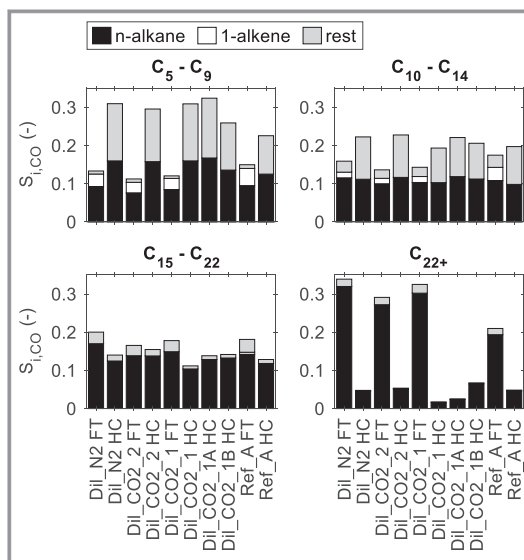


**Figure 6.** Integral CO-related hydrocarbon selectivity of product lumps for FT and FT-HC measurements (Tab. 1, Tab. 2). In FT products,  $n$ -alkanes and 1-alkenes could be distinguished; in FT-HC products, only  $n$ -alkanes could be distinguished with the GC analysis at hand.

sion effect on wax/gas ratio) and the analysis at hand. A more detailed analysis of the HC products would require GC×GC analysis.

### 3.3 Variation of HC Conditions

To enhance the kerosene selectivity at the expense of naphtha production, the conditions in the HC were varied. Additional  $H_2$  feed (Dil\_CO2\_1A compared to Dil\_CO2\_1) as suggested by Freitez et al. [38] did neither exhibit a remarkable influence on kerosene and naphtha selectivity nor on mass distribution or average chain length (Fig. 6, Fig. 8, Tab. 5). The wax conversion decreased slightly under  $H_2$  addition. Due to the higher  $H_2$  partial pressure, the dehydrogenation/hydrogenation equilibrium shifts towards hydro-

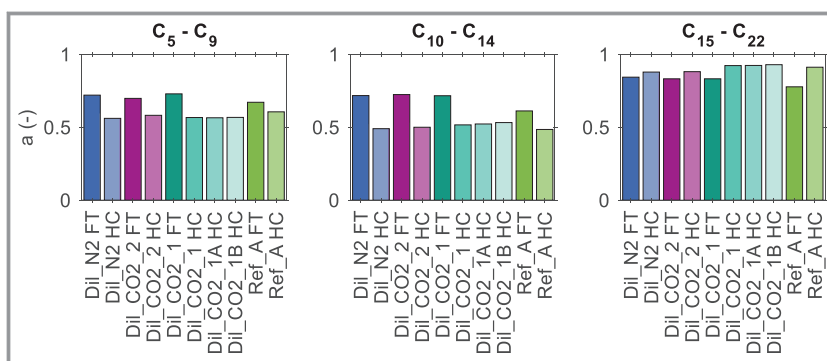


**Figure 7.** Integral  $n$ -alkane fraction (Eq. (10)) of product lumps for FT and FT-HC measurements (Tab. 1, Tab. 2).

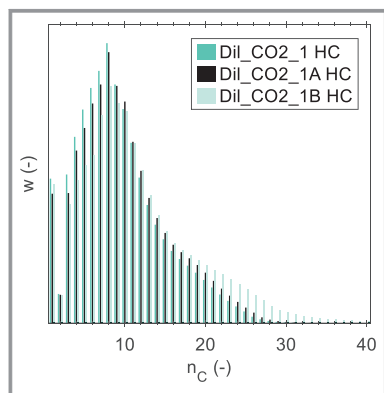


**Figure 8.** Hydrocarbon mass fractions for coupled FT-HC measurements with varying HC conditions (Tab. 2). FT feed: 38.8 % H<sub>2</sub>, 19.4 % CO, 38.8 % CO<sub>2</sub>, 3.0 % N<sub>2</sub>,  $WHSV_{FT} = 4.5 \text{ h}^{-1}$ .

genation. This gives rise to the assumption that less dehydrogenation of long-chain alkanes as cracking initiation step occurred, and higher hydrogen partial pressure is inhibiting this step. The hydrogenation functionality is further influenced by the considerably high CO content.

**Table 5.** Experimental wax (C<sub>22+</sub>) conversion in coupled FT-HC measurements and average chain length for FT and FT-HC measurements with varying HC conditions (Tabs. 1 and 2).

	$X_{C_{22+}}$ [%]	$\bar{n}_{C,FT}$ [-]	$\bar{n}_{C,HC}$ [-]
Dil_CO2_1	94.8	20	9
Dil_CO2_1A	92.6	20	10
Dil_CO2_1B	79.0	20	11

To further decrease the wax conversion in the HC, the catalyst mass was reduced from Dil\_CO2\_1A to Dil\_CO2\_1B. Fig. 8 shows the weight distribution of the C-species as function of the C-number while varying the HC conditions only. The figure indicates that the fractions of hydrocarbons with more than 11 carbon atoms are higher with decreasing catalyst mass. A lower wax conversion seems to be beneficial to avoid over-cracking.

The investigated variations of the HC operating conditions did not lead to any change in the *n*-alkane fraction (Fig. 7). A more complex process design including wax recycling is therefore commissioned in the Kerogreen process chain to reduce the consumption of the gas oil fraction and to improve the kerosene selectivity. The proof of the beneficial conditions in a liquid-rich HC step is nevertheless pending by future work.

### 3.4 Carbonaceous Species in the Water Phase

Besides hydrocarbons, also oxygenates, mainly alcohols and traces of carboxylic acids, are produced in Co-LTFT. Primary alcohols with up to five carbon atoms dissolve selectively in the aqueous phase, whereas long-chain alcohols aggregate in the oil fraction [10].

Fig. 9a displays the alcohol mass fractions of methanol, ethanol, 1-propanol up to 1-pentanol in the water phase collected in the cold trap at 10 °C for FT reference measurements. The values range from 0.5 wt % (methanol) to less than 0.1 wt % (1-pentanol). In coupled FT-HC operation mode, oxygenates of the FT product reacted further on the bifunctional HC catalyst. Fig. 9b shows the conversion of alcohols in the HC stage. From this graph, it can be seen that the decrease of mass fraction after HC was more pronounced for long-chain alcohols and accounted for around 25 to 50 % for methanol, and more than 80 % for 1-pentanol.

To the best of the authors' knowledge, no research has been published on the aqueous phase oxygenates reactions of FT products directly converted on HC catalysts. Depending on the hydrogen partial pressure and prevailing reaction conditions, potential reactions could involve dehydroxylation and hydrogenation steps. The former being catalyzed on Brønstedt-active acidic sites, the latter on the Pt sites of the catalyst.

In Fig. 9b, no clear relation between alcohol conversion and CO<sub>2</sub> content in the syngas feed is observed. Reasonable trends for the variation of HC conditions could be distinguished: first, additional H<sub>2</sub> feed in the HC resulted in smaller alcohol conversion. This effect could either be attributed to the lower residence time or indicate that hydrogenation is not solely responsible for oxygenate reactions on the bifunctional catalyst. Second, as expected, less catalyst mass led to smaller conversion of alcohols. These results show that FT syncrude upgrading by means of directly coupled HC reduces the loss of carbonaceous species to the water phase.

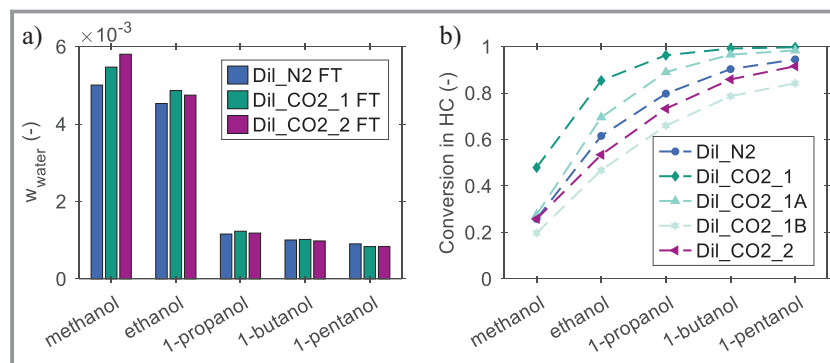


**Figure 9.** C<sub>1</sub>–C<sub>5</sub> alcohols in the water phase collected in the cold trap at 10 °C. a) Mass fractions in water phase for FT reference measurements. b) Conversion of alcohols in the HC for FT-HC measurements.



## 4 Conclusions

This experimental study investigated the influence of CO<sub>2</sub>-rich syngas feeds on the product distribution of combined FT-HC operation. Therefore, syngas with and without CO<sub>2</sub> was used as feed for solely FT and coupled FT-HC experiments. Commercial catalysts were employed: cobalt-based in the FT, and Pt/H-ZSM in the HC. The product distribution was obtained from gas, oil (collected at 10 °C), and wax (collected at 180 °C) phase analysis. Additionally, the oxygenates dissolved in the water phase were analyzed.

The FT reference measurements (without HC) confirmed that CO<sub>2</sub> does not influence the FT product distribution and can be treated as an inert gas. The product distribution for C<sub>10</sub>–C<sub>50</sub> could be well described according to the ASF model with an average chain growth probability of 0.91.

The coupled FT-HC experiments showed that mainly the wax fraction and parts of the gas oil fraction were selectively converted to kerosene and naphtha range hydrocarbons during HC. Linear FT alkanes were either isomerized or dehydrogenated and a limited hydrocarbon net production of C<sub>14</sub> was revealed. As no significant difference between the syngas with N<sub>2</sub> and CO<sub>2</sub> was detected, the effects of CO<sub>2</sub> in the coupled FT-HC process seem to be negligible. Although the FT-HC product is rich in kerosene substitute starting material, the loss of gas oil should be lowered in a compact FT-HC process. A recycling of wax may be straightforward to lower the wax conversion per pass, thus, keeping CO away from the catalyst surface and lowering conversion. This will be tested in the future in the Kerogreen plant.

Interestingly, it was found that alcohols (C<sub>1</sub>–C<sub>5</sub>) dissolved in the FT water phase reacted further on the bifunctional HC catalyst. Although no clear relation between the CO<sub>2</sub> content in the syngas and the alcohol conversion could be deduced, a clear trend was visible for the alcohol conversion in dependence of the alcohol chain length.

The experimental results show that FT syncrude upgrading by means of direct HC is not remarkably influenced by the CO<sub>2</sub> content in the syngas feed. Nevertheless, the diluting effect has to be considered for the reactor design. Therefore, the investigated Kerogreen process route seems to be an interesting case study in the PtL framework.

The authors would like to thank Florian Mian for experimental and Daniel Hodonj for experimental and analytical support. The work presented in this paper is part of the European project Kerogreen, which has received funding from the European Union's Horizon 2020 research and innovation programme under grant agreement no. 763909. Open access funding enabled and organized by Projekt DEAL.

## Symbols

$a$	[-]	$n$ -alkane fraction
$m$	[g]	mass
$\dot{m}$	[g h <sup>-1</sup> ]	mass flow rate
$\dot{n}$	[mol h <sup>-1</sup> ]	molar flow rate
$n_C$	[-]	carbon number
$\bar{n}_C$	[-]	average chain length
$S$	[-]	selectivity
$w$	[-]	mass fraction
$WHSV$	[h <sup>-1</sup> ]	weight hourly space velocity
$X$	[-]	conversion
$\alpha$	[-]	chain growth probability

## Sub- and superscripts

cat	catalyst
CO	carbon monoxide
exp	experimental value
FT	Fischer-Tropsch
HC	hydrocracking
$i$	hydrocarbon chain length
in	reactor inlet
out	reactor outlet
sim	simulated value

## Abbreviations

ASF	Anderson-Schulz-Flory distribution
Co-LTFT	low temperature Fischer-Tropsch on cobalt catalyst
FID	flame ionization detector
FT	Fischer-Tropsch
FT-HC	Fischer-Tropsch coupled with hydrocracking
GC	gas chromatograph
HC	hydrocracking
PtL	Power-to-Liquid
SEWGS	sorption-enhanced water-gas shift
syncrude	Fischer-Tropsch crude product
syngas	synthesis gas (CO + H <sub>2</sub> )
TCD	thermal conductivity detector
TOS	time-on-stream

## References

- [1] *A European Strategy for Low-Emission Mobility*, European Commission, Brussels 2016. <https://eur-lex.europa.eu/legal-content/en/TXT/?uri=CELEX:52016DC0501>
- [2] A. P. H. Goede, *EPJ Web Conf.* **2018**, 189, 00010. DOI: <https://doi.org/10.1051/epjconf/201818900010>
- [3] P. Viegas, L. Vialto, A. J. Wolf, F. J. J. Peeters, P. W. C. Groen, T. W. H. Righart, W. A. Bongers, M. C. M. van de Sanden, P. Diomedea, *Plasma Sources Sci. Technol.* **2020**, 29 (10), 105014. DOI: <https://doi.org/10.1088/1361-6595/abb41c>

- [4] T. J. Stadler, P. Barbig, J. Kiehl, R. Schulz, T. Klövekorn, P. Pfeifer, *Energies* **2021**, *14* (2), 355. DOI: <https://doi.org/10.3390/en14020355>
- [5] A. Ramirez, S. M. Sarathy, J. Gascon, *Trends Chem.* **2020**, *2* (9), 785–795. DOI: <https://doi.org/10.1016/j.trechm.2020.07.005>
- [6] H. Kirsch, N. Lochmahr, C. Staudt, P. Pfeifer, R. Dittmeyer, *Chem. Eng. J.* **2020**, *393*, 124553. DOI: <https://doi.org/10.1016/j.cej.2020.124553>
- [7] S. Jürgens, P. Oßwald, M. Selinsek, P. Piermartini, J. Schwab, P. Pfeifer, U. Bauder, S. Ruoff, B. Rauch, M. Köhler, *Fuel Process. Technol.* **2019**, *193*, 232–243. DOI: <https://doi.org/10.1016/j.fuproc.2019.05.015>
- [8] A. de Klerk, in *Fischer-Tropsch Synthesis, Catalysts, and Catalysis: Advances and Applications* (Eds: B. H. Davis, M. L. Occelli), Chemical Industries, Vol. 142, CRC Press, Boca Raton, FL **2016**.
- [9] D. Chakrabarti, V. Prasad, A. de Klerk, in *Fischer-Tropsch Synthesis, Catalysts, and Catalysis: Advances and Applications* (Eds: B. H. Davis, M. L. Occelli), Chemical Industries, Vol. 142, CRC Press, Boca Raton, FL **2016**.
- [10] A. de Klerk, *Fischer-Tropsch Refining*, Wiley-VCH, Weinheim **2011**.
- [11] R. B. Anderson, R. A. Friedel, H. H. Storch, *J. Chem. Phys.* **1951**, *19* (3), 313–319. DOI: <https://doi.org/10.1063/1.1748201>
- [12] P. J. Flory, *J. Am. Chem. Soc.* **1936**, *58* (10), 1877–1885. DOI: <https://doi.org/10.1021/ja01301a016>
- [13] F. G. Botes, L. P. Dancuart, H. G. Nel, A. P. Steynberg, A. P. Vogel, B. B. Breman, J. Font Freide, in *Advances in Clean Hydrocarbon Fuel Processing*, Woodhead Publishing, Cambridge **2011**.
- [14] A. de Klerk, *Energy Environ. Sci.* **2011**, *4* (4), 1177. DOI: <https://doi.org/10.1039/c0ee00692k>
- [15] J. Weitkamp, *ChemCatChem* **2012**, *4* (3), 292–306. DOI: <https://doi.org/10.1002/cctc.201100315>
- [16] C. Sun, T. Zhan, P. Pfeifer, R. Dittmeyer, *Chem. Eng. J.* **2017**, *310*, 272–281. DOI: <https://doi.org/10.1016/j.cej.2016.10.118>
- [17] T. Hanaoka, T. Miyazawa, K. Shimura, S. Hirata, *Chem. Eng. J.* **2015**, *263*, 178–185. DOI: <https://doi.org/10.1016/j.cej.2014.11.042>
- [18] C. G. Visconti, L. Lietti, E. Tronconi, P. Forzatti, R. Zennaro, E. Finocchio, *Appl. Catal., A* **2009**, *355* (1–2), 61–68. DOI: <https://doi.org/10.1016/j.apcata.2008.11.027>
- [19] M. K. Gnanamani, W. D. Shafer, D. E. Sparks, B. H. Davis, *Catal. Commun.* **2011**, *12* (11), 936–939. DOI: <https://doi.org/10.1016/j.catcom.2011.03.002>
- [20] Y. Yao, X. Liu, D. Hildebrandt, D. Glasser, *Chem. Eng. J.* **2012**, *193–194*, 318–327. DOI: <https://doi.org/10.1016/j.cej.2012.04.045>
- [21] A. H. Lillebø, A. Holmen, B. C. Enger, E. A. Blekkan, *Wiley Interdiscip. Rev.: Energy Environ.* **2013**, *2* (5), 507–524. DOI: <https://doi.org/10.1002/wene.69>
- [22] H. Kirsch, L. Brübach, M. Loewert, M. Riedinger, A. Gräfenhahn, T. Böltken, M. Klumpp, P. Pfeifer, R. Dittmeyer, *Chem. Ing. Tech.* **2020**, *92* (1–2), 91–99. DOI: <https://doi.org/10.1002/cite.201900120>
- [23] R. Dittmeyer, P. Pfeifer, K. Schubert, *EP2617487 (A1)*, **2013**.
- [24] P. Pfeifer, P. Piermartini, A. Wenka, *DE102015111614 (A1)*, **2015**.
- [25] K. Dettmer-Wilde, W. Engewald, *Practical Gas Chromatography*, Springer, Berlin **2014**.
- [26] W. Shafer, M. Gnanamani, U. Graham, J. Yang, C. Masuku, G. Jacobs, B. Davis, *Catalysts* **2019**, *9* (3), 259. DOI: <https://doi.org/10.3390/catal9030259>
- [27] C. G. Visconti, E. Tronconi, L. Lietti, R. Zennaro, P. Forzatti, *Chem. Eng. Sci.* **2007**, *62* (18–20), 5338–5343. DOI: <https://doi.org/10.1016/j.ces.2006.12.064>
- [28] P. Piermartini, T. Böltken, M. Selinsek, P. Pfeifer, *Chem. Eng. J.* **2017**, *313*, 328–335. DOI: <https://doi.org/10.1016/j.cej.2016.12.076>
- [29] R. Yang, L. Zhou, J. Gao, X. Hao, B. Wu, Y. Yang, Y. Li, *Catal. Today* **2017**, *298*, 77–88. DOI: <https://doi.org/10.1016/j.cattod.2017.05.056>
- [30] J. Gao, B. Wu, L. Zhou, Y. Yang, X. Hao, J. Xu, Y. Xu, Y. Li, *Ind. Eng. Chem. Res.* **2012**, *51* (36), 11618–11628. DOI: <https://doi.org/10.1021/ie201671g>
- [31] Y. Lu, T. Lee, *J. Nat. Gas Chem.* **2007**, *16* (4), 329–341. DOI: [https://doi.org/10.1016/S1003-9953\(08\)60001-8](https://doi.org/10.1016/S1003-9953(08)60001-8)
- [32] T. Riedel, M. Claeys, H. Schulz, G. Schaub, S.-S. Nam, K.-W. Jun, M.-J. Choi, G. Kishan, K.-W. Lee, *Appl. Catal., A* **1999**, *186* (1–2), 201–213. DOI: [https://doi.org/10.1016/S0926-860X\(99\)00173-8](https://doi.org/10.1016/S0926-860X(99)00173-8)
- [33] C. L. Tucker, E. van Steen, *Catal. Today* **2020**, *342*, 115–123. DOI: <https://doi.org/10.1016/j.cattod.2018.12.049>
- [34] C. G. Visconti, M. Martinelli, L. Falbo, L. Fratolocchi, L. Lietti, *Catal. Today* **2016**, *277*, 161–170. DOI: <https://doi.org/10.1016/j.cattod.2016.04.010>
- [35] Y. Zhang, G. Jacobs, D. E. Sparks, M. E. Dry, B. H. Davis, *Catal. Today* **2002**, *71* (3–4), 411–418. DOI: [https://doi.org/10.1016/S0920-5861\(01\)00468-0](https://doi.org/10.1016/S0920-5861(01)00468-0)
- [36] R. Brosius, J. C. Fletcher, *J. Catal.* **2014**, *317*, 318–325. DOI: <https://doi.org/10.1016/j.jcat.2014.07.004>
- [37] R. Brosius, P. J. Kooyman, J. C. Q. Fletcher, *ACS Catal.* **2016**, *6* (11), 7710–7715. DOI: <https://doi.org/10.1021/acscatal.6b02223>
- [38] A. Freitez, K. Pabst, B. Kraushaar-Czarnetzki, G. Schaub, *Ind. Eng. Chem. Res.* **2011**, *50* (24), 13732–13741. DOI: <https://doi.org/10.1021/ie201913s>